Hindawi Publishing Corporation
International Journal of Antennas and Propagation
Volume 2015, Article ID 439832, 7 pages
http://dx.doi.org/10.1155/2015/439832

Research Article

Dual Band-Notched Microstrip-Fed Vivaldi Antenna Utilizing Compact EBG Structures

K. A. Alshamaileh, M. J. Almalkawi, and V. K. Devabhaktuni

Electrical Engineering and Computer Science Department, University of Toledo, 2801 W. Bancroft Street, Toledo, OH 43606, USA

Correspondence should be addressed to M. J. Almalkawi; mohammad.almalkawi@utoledo.edu

Received 5 January 2015; Revised 2 February 2015; Accepted 2 February 2015

Academic Editor: Claudio Gennarelli

We propose an ultra-wideband (UWB) antipodal Vivaldi antenna (AVA) with high-Q stopband characteristics based on compact electromagnetic bandgap (EBG) structures. First, an AVA is designed and optimized to operate over an UWB spectrum. Then, two pairs of EBG cells are introduced along the antenna feed line to suppress the frequency components at 3.6–3.9 and 5.6–5.8 GHz (i.e., WiMAX and ISM bands, resp.). Simulated and measured results show a voltage standing wave ratio (VSWR) below 2 for the entire 3.1–10.6 GHz band with high attenuation at the two selected subbands. This simple yet effective approach eliminates the need to deform the antenna radiators with slots/parasitic elements or comprise multilayer substrates. Furthermore, the flexibility it offers in terms of controlling both the number and locations of the band-reject frequencies is advantageous for antennas with nonuniform flares as in the AVA.

1. Introduction

Researchers all over the globe are in harmony when it comes to the significance of the antipodal Vivaldi antenna (AVA) in the field of ultra-wideband (UWB) communications owing to its broadband frequency characteristics, low thermal noise, high gain, and directive radiation [1]. Because of these desirable electrical features, such an antenna proved to be a competitive candidate for several applications including medical microwave imaging and radar telemetry [2]. The broadband performance of AVAs, however, may cause considerable interference to other coexisting wireless technologies and thus negatively affect their intended functions. Although planar antennas with narrow stopband characteristics have been extensively investigated [3–7], little efforts have been done to mitigate interference between AVAs and other wireless technologies, basically due to the nonuniformity of the AVA radiators which follows either an exponential or elliptical taper. In addition, their relatively low current distribution makes it difficult for antenna designers to drive the structure towards exhibiting frequency notch(s). Recent research articles have reported several band-reject resonators to alleviate the interference impact mainly through one of the following techniques: (1) etched slots on the antenna radiators [8, 9] and (2) parasitic elements on the radiation surface [10]. In [8], an Ω-shaped slot was made in each radiating flare to create a frequency notch at 5.5 GHz. Following a similar approach, [9] proposed an AVA with a U-shaped slot to realize a band-notch at the same frequency. This technique was also applied to different antennas in order to obtain notches at predefined stopbands [3, 4]. It is noteworthy that apertures excavating techniques reported in [8, 9] require extensive parametric simulations and may degrade antenna gain due to copper etching [11]. The concept of applying split ring resonators (SRRs) as parasitic elements on the radiation surface was applied in [10] to create a notch within the 5-6 GHz band. Similar concept was applied in [5] taking into account a different antenna structure, in which a triple-notched UWB antenna was designed using three parasitic strips accompanied with a deformed ground plane. Besides the increased computational demand, approaches in [5, 10] negatively impact the overall design complexity. Other efforts incorporated multilayers stacked together to achieve multiple band-notches. In [6, 7], stopband resonators in multilayer configurations have been introduced. Nevertheless, the increase in the fabrication cost and structural complexity and assembly are major drawbacks.

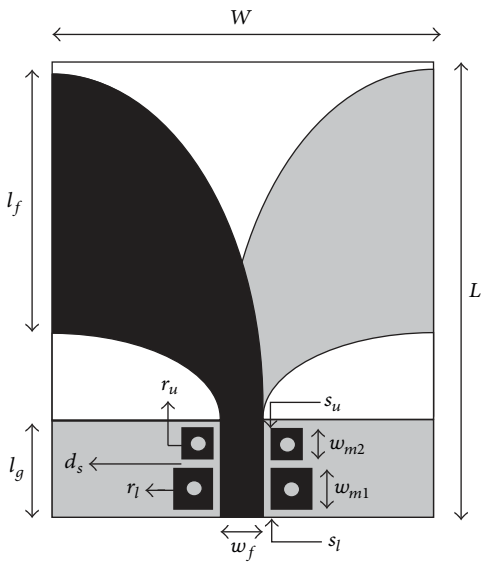

Design variables (mm):

W (substrate width)	66.3	l_g (ground length)	18
L (substrate length)	66.3	r_u (via radius)	0.4
w_f (feed line width)	2.7	r_l (via radius)	0.3
w_{m1} (EBG$_1$ width)	9.3	s_l (EBG$_1$ to feed line)	0.2
w_{m2} (EBG$_2$ width)	7	s_u (EBG$_2$ to feedl ine)	0.4
l_f (max. flare width)	47.4	d_s (EBG$_1$ to EBG$_2$)	0.45

Figure 1: Proposed AVA: black and gray strips refer to upper and lower flares, respectively.

In this paper, we propose a double narrowband-notch AVA with an excellent rejection level at the notch bands without disfiguring the radiating flares or utilizing multilayered substrates to realize the intended notches. The design concept offers flexibility in terms of controlling the number and locations of the band-reject frequencies, especially for antennas with nonuniform radiators as in the AVA.

2. Antenna Configuration

Considering a characteristic impedance of 50-Ω, Rogers RO4003C substrate with relative permittivity of 3.55, thickness of 0.813 mm, and loss tangent of 0.0027, the layout of the proposed antenna along with the associating dimensions is illustrated in Figure 1. In this design, two pairs of mushroom-like EBG cells surround the antenna feed line. The frequency notches $f_i = 1/2\pi\sqrt{L_iC_i}$, where $i = 1, 2$, are fundamentally due to the inductance L_i that results from the current flowing through the vias and the capacitance C_i established from the gap between the cells' top patches and the ground plane. It should be pointed out here that the AVA's flares are of an elliptical taper with design equations derived in [12].

3. Performance Analysis

The proposed design is analyzed to demonstrate its capability in controlling the notches locations by modifying the parameters of each EBG pair. For the sake of brevity, the lower pair

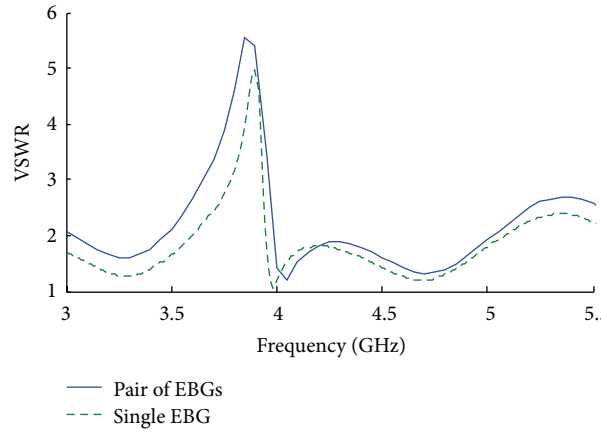

Figure 2: Notch characteristics for pair and single EBG cells.

(EBG$_1$) is considered in this study; though same conclusions hold for the upper pair (EBG$_2$). Figure 2 represents the notch characteristics in the case of utilizing the lower pair versus a single EBG cell (the one either on right or left). It is observed that incorporating two EBG cells around the feed line increases the notch bandwidth by 10% as compared to one cell. Furthermore, the rejection level in the former is higher.

Figure 3 shows the effect of changing the radius r_l, width w_{m1}, and the separation distance s_l on the notch location. Increasing r_l (Figure 3(a)) results in reducing the inductance L_1 [13, equation 1]. Thus, a positive shift occurs in f_1. Similarly, increasing r_u reduces L_2, which results in an increase of f_2. On the other hand, increasing w_{m1} (Figure 3(b)) increases C_1 which reduces f_1. Alike w_{m1}, increasing w_{m2} increases C_2, which in turn reduces f_2. Figure 3(c) shows the effect of varying s_l on the antenna response. The closer EBG$_i$ is to the feed line, the sharper the notch f_i will be due to the increased coupling level between EBGs' patches and the feed line, with no significant effect on the notches positions. Figure 4 depicts the minor influence of varying d_s separating the two EBG pairs on the resulting VSWR, justifying the negligible cross coupling among both pairs, EBG$_1$ and EBG$_2$. It is paramount to point out that the concept of EBG cells was applied to introduce frequency notches in UWB monopole antennas [14–16].

4. Results and Discussion

Figure 5 illustrates the voltage standing wave ratio (VSWR) for four different simulation studies. First, an AVA is optimized to operate over the UWB frequency range. Then, two pairs of EBGs, lower and upper, are incorporated in the design, one pair at a time, to achieve a frequency notch at the 3.6–3.9 and 5.6–5.8 GHz bands, respectively. Finally, the antenna is simulated utilizing the two EBG pairs (considering the dimensions reported in Figure 1) to obtain the two predefined stopbands. As can be noticed, the conventional design, without EBG cells, shows a VSWR < 2 in the frequency range 3.1–10.6 GHz. On the other hand, incorporating only

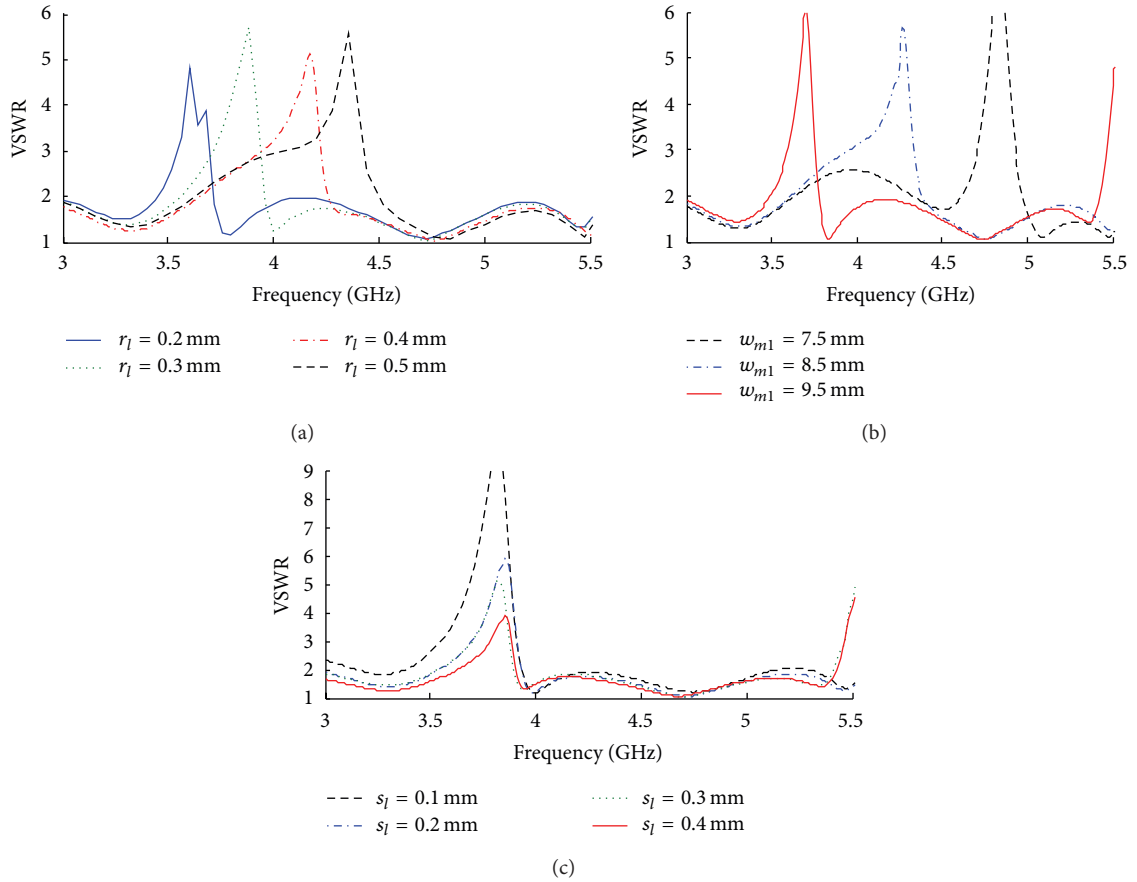

FIGURE 3: Effect of changing EBG_1 (a) radius r_l, (b) width w_{m1}, and (c) s_l.

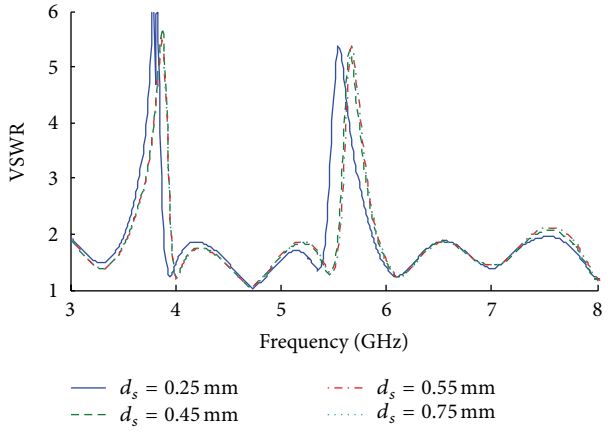

FIGURE 4: VSWR simulations for four different d_s values.

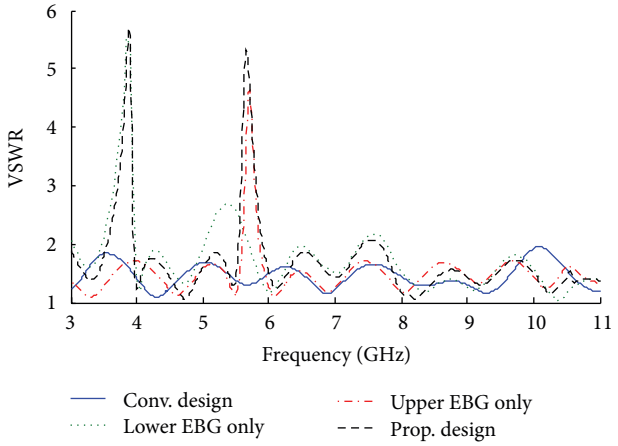

FIGURE 5: AVA VSWR simulation results for four different scenarios.

the lower EBG pair results in a VSWR $<$ 2 over the UWB range except for the 3.6–3.9 GHz band (VSWR = 5.8). Similarly, the upper EBG pair produces an UWB response except for the 5.6–5.8 GHz band, which possesses a VSWR of 5.4. Finally, concatenating the two EBG pairs generates two simultaneous notches at the 3.6–3.9 and 5.6–5.8 GHz frequencies with VSWR values of 5.8 and 5.4, respectively, and less than 2 elsewhere. Hence, the easiness of controlling each notch without affecting the other is achieved owing to the low cross coupling between the incorporated EBG elements. Although AVA flares have a bulky size, EBG cells with electrically small dimensions are more than enough to introduce high Q reject bands.

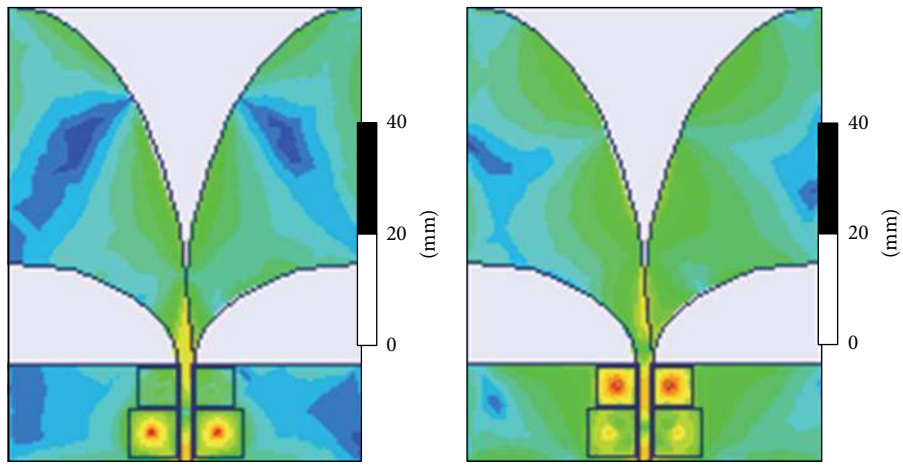

Figure 6: Current distribution of the proposed dual-notch AVA at (a) 3.8 GHz and (b) 5.7 GHz.

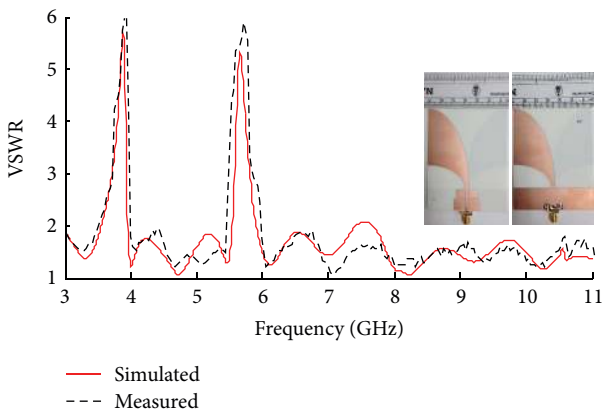

Figure 7: Simulated and measured VSWRs of the proposed AVA.

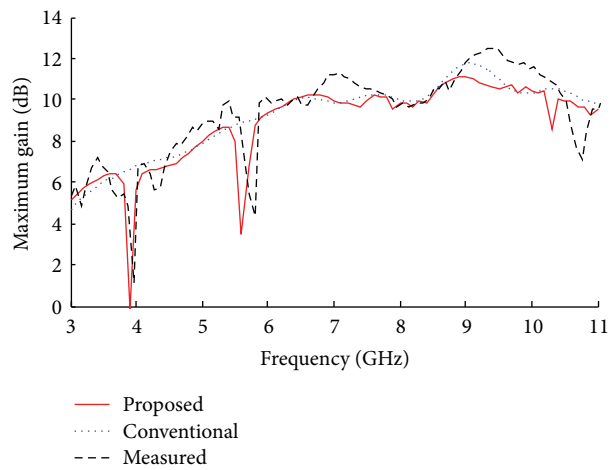

Figure 8: Peak gain for both conventional and proposed AVAs.

The current distribution of the antenna is depicted in Figure 6. As can be seen, the lower EBG pair is activated around 3.8 GHz, while the upper one is activated at 5.7 GHz creating band notches (i.e., bandgaps) at these frequencies.

The measured VSWR, radiation patterns, peak gain, and group delay of the fabricated AVA prototype with band-notch characteristics at 3.6–3.9 and 5.6–5.8 GHz are presented and compared with those obtained by simulations. The VSWR is measured after a two-port calibration to a Rhode & Schwarz ZVB20 vector network analyzer (VNA) and is illustrated in Figure 7. Simulated and measured results are in good agreement with a clear frequency-reject performance at the intended bands with discrepancies thought to be due to fabrication tolerances. Figure 8 shows the measured conventional and proposed AVAs gain over the UWB spectrum using two identical antennas separated by a distance $d = 1.25$ m. The measured transmission coefficient is applied to calculate the antenna gain utilizing the equation [17]:

$$|S_{21}|^2 = G_T G_R \frac{\lambda}{(4\pi d)^2}, \quad (1)$$

where G_T and G_R are the gains of the transmitter and receiver, respectively, and λ is the free space wavelength in meters. As shown in Figure 8, an excellent gain suppression of 7 dB and 5.4 dB is obtained at the first and second notches, respectively.

Simulated and measured far-field radiation patterns of the proposed antenna at different frequencies are shown in Figure 9. As can be seen in Figures 9(a)–9(c), the proposed AVA maintained its directive radiation with no pattern distortion as their corresponding frequencies (5, 7, and 9 GHz) are distant from the notches locations. However, clear pattern distortion and gain attenuation appear in Figures 9(d) and 9(e) as they express the antenna radiation at 3.8 and 5.7 GHz, respectively, (i.e., within the reject-bands). Figure 10 illustrates the measured group delay of the proposed AVA. To measure such a parameter, two identical antennas were placed 1.25 m apart, and S_{21} was recorded with a suitable

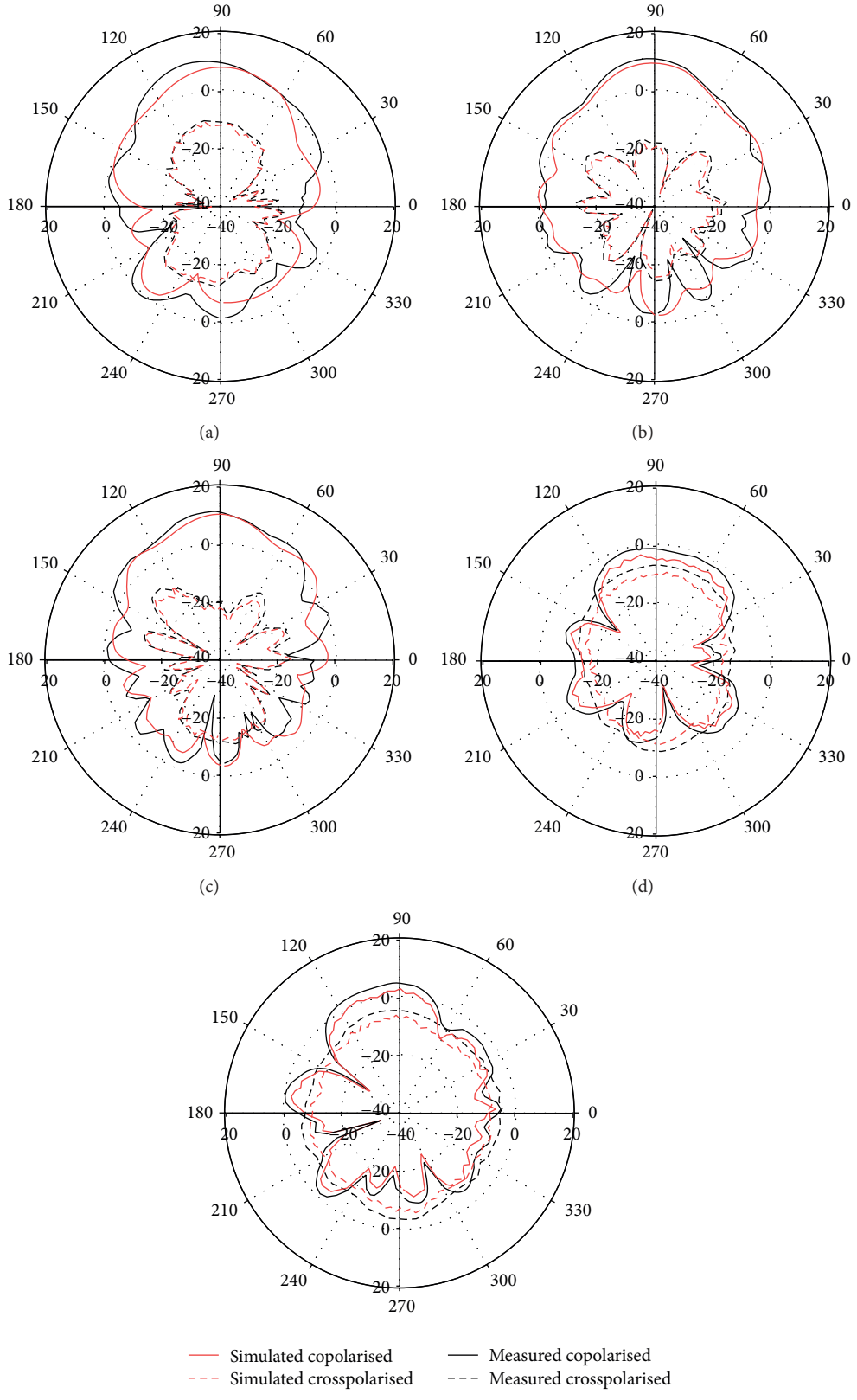

Figure 9: Proposed dual band-notched AVA radiation pattern: (a) 5 GHz, (b) 7 GHz, (c) 9 GHz, (d) 3.8 GHz, center frequency of the 1st notch, and (e) 5.7 GHz, center frequency of the 2nd notch.

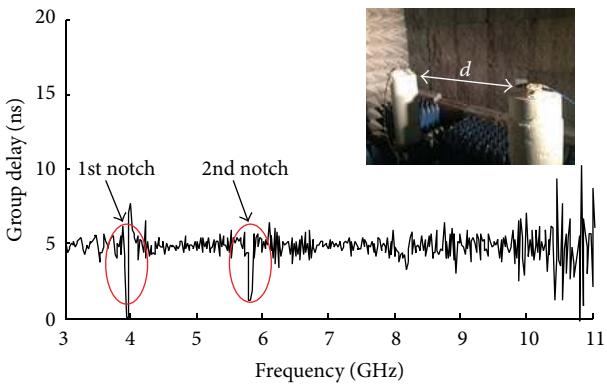

FIGURE 10: Measured group delay of the proposed antenna.

frequency step size f_i. Finally, the group delay (τ) is calculated by the following equation [18]:

$$\tau = -\frac{\Delta\theta}{360\Delta f}, \quad (2)$$

where $\Delta\theta = \theta_{fi} - \theta_{fi-1}$ is S_{21} phase difference of $(\theta_{fi}, \theta_{fi-1})$, and $\Delta f = f_i - f_{i-1}$. As seen in Figure 10, the measured group delay is almost flat over the UWB range (around 5 ns), which reflects an acceptable linearity between phase and frequency components for the whole band except the two notches showing τ of 0.1 ns and 0.9 ns at f_1 and f_2, respectively. The small τ fluctuation elsewhere is mainly due to various measurement dispersion mechanisms (e.g., cable dispersion).

5. Conclusion

An UWB AVA with high-Q dual rejection bands incorporating mushroom-like EBG cells was presented. Adjoining two pairs of EBG structures to the antenna feed line lead to two bandgaps. For verification purposes, an AVA with band-notches at 3.8 and 5.7 GHz was designed, simulated, and measured. The good agreement between both simulation and measurement results proves the concept of utilized EBG elements. The proposed approach is advantageous for antennas with nonuniform flares and flexible in controlling both the number and locations of the frequency notches. Ease of fabrication and excellent electrical performance provide a competitive design that fits many wireless applications.

Conflict of Interests

The authors declare that there is no conflict of interests regarding the publication of this paper.

Acknowledgment

This work was supported by NSF EARS Award 1247946 (Program Director George Haddad).

References

[1] E. Gazit, "Improved design of the Vivaldi antenna," *Proceedings of the Institution of Electrical Engineering*, vol. 135, no. 2, pp. 89–92, 1988.

[2] C. Li, X. Lin, P. Tang, and S. Luo, "An antipodal vivaldi antenna for ultra wideband medical imaging system," in *Proceedings of the 3rd IEEE International Workshop on Electromagnetics: Applications and Student Innovation Competition (iWEM '12)*, pp. 1–2, Sichuan, China, August 2012.

[3] D. T. Nguyen, D. H. Lee, and H. C. Park, "Very compact printed triple band-notched UWB antenna with quarter-wavelength slots," *IEEE Antennas and Wireless Propagation Letters*, vol. 11, pp. 411–414, 2012.

[4] N. Tasouji, J. Nourinia, C. Ghobadi, and F. Tofigh, "A novel printed UWB slot antenna with reconfigurable band-notch characteristics," *IEEE Antennas and Wireless Propagation Letters*, vol. 12, pp. 922–925, 2013.

[5] M. T. Islam, R. Azim, and A. T. Mobashsher, "Triple band-notched planar UWB antenna using parasitic strips," *Progress in Electromagnetics Research*, vol. 129, pp. 161–179, 2012.

[6] Y. D. Dong, W. Hong, Z. Q. Kuai et al., "Development of ultrawideband antenna with multiple band-notched characteristics using half mode substrate integrated waveguide cavity technology," *IEEE Transactions on Antennas and Propagation*, vol. 56, no. 9, pp. 2894–2902, 2008.

[7] M. Almalkawi and V. Devabhaktuni, "Ultrawideband antenna with triple band-notched characteristics using closed-loop ring resonators," *IEEE Antennas and Wireless Propagation Letters*, vol. 10, pp. 959–962, 2011.

[8] K. A. Reddy, S. Natarajamani, and S. K. Behera, "Antipodal vivaldi antenna UWB antenna with 5.5 GHz band-notch characteristics," in *Proceedings of the International Conference on Computing, Electronics and Electrical Technologies (ICCEET '12)*, pp. 821–824, ind, March 2012.

[9] M. John, M. J. Ammann, and P. McEvoy, "UWB Vivaldi antenna based on a spline geometry with frequency band-notch," in *Proceedings of the IEEE International Symposium on Antennas and Propagation*, pp. 1–4, San Diego, Calif, USA, July 2008.

[10] D. Sarkar and K. V. Srivastava, "SRR-loaded antipodal Vivaldi antenna for UWB applications with tunable notch function," in *Proceedings of the 21st International Symposium on Electromagnetic Theory (EMTS '13)*, pp. 466–469, Hiroshima, Japan, May 2013.

[11] G. Clasen and R. Langley, "Meshed patch antennas," *IEEE Transactions on Antennas and Propagation*, vol. 52, no. 6, pp. 1412–1416, 2004.

[12] A. M. Abbosh, H. K. Kan, and M. E. Bialkowski, "Design of compact directive ultra wideband antipodal antenna," *Microwave and Optical Technology Letters*, vol. 48, no. 12, pp. 2448–2450, 2006.

[13] M. Rahman and M. A. Stuchly, "Transmission line-periodic circuit representation of planar microwave photonic bandgap structures," *Microwave and Optical Technology Letters*, vol. 30, no. 1, pp. 15–19, 2001.

[14] L. Peng and C.-L. Ruan, "UWB band-notched monopole antenna design using electromagnetic-bandgap structures," *IEEE Transactions on Microwave Theory and Techniques*, vol. 59, no. 4, pp. 1074–1081, 2011.

[15] T. Li, H.-Q. Zhai, G.-H. Li, and C.-H. Liang, "Design of compact UWB band-notched antenna by means of electromagnetic-

bandgap structures," *Electronics Letters*, vol. 48, no. 11, pp. 608–609, 2012.

[16] M. Yazdi and N. Komjani, "Design of a band-notched UWB monopole antenna by means of an EBG structure," *IEEE Antennas and Wireless Propagation Letters*, vol. 1, pp. 170–173, 2011.

[17] J. Glimm, R. Harms, K. Münter, M. Spitzer, and R. Pape, "A single-antenna method for traceable antenna gain measurement," *IEEE Transactions on Electromagnetic Compatibility*, vol. 41, no. 4, pp. 436–439, 1999.

[18] CJS Labs, San Francisco, Calif, USA, http://www.cjs-labs.com/.